

EXTRACTING DYNAMIC RESISTANCE FROM A PULSED POWER SWITCH WITH A LEAST SQUARES APPROACH

F.J. Zutavern^{1*}, S.F. Glover¹, A.P. Mancuso¹,
P.J. Foster², F.E. White³,

¹*Sandia National Laboratories, Albuquerque, NM 87185 USA*

²*Defense Nuclear Facilities Safety Board, Washington, DC 20004 USA*

³*Science Applications International Corporation, Albuquerque, NM 87106 USA*

Abstract

Pulsed power gas switches operate under extreme conditions holding off voltages at millions of volts and greater, conducting currents at 100's of kiloamps, and can reliably trigger with less than 10ns of jitter at optimal operating conditions. However as Martin and Braginskii had noted the impedance of these switches is dynamic and a function of many parameters such as gas pressure, current, and the number of channels. In systems such as Protogen or Ursa Minor many gas switches are utilized to enable optimal performance and pulse shaping. A challenge with either system is that, if the switches are tightly coupled and one switch triggers early, then the fields on the second switch change dramatically and can move the second switch into a new operating regime that will result in a different dynamic resistance. This paper presents a least squares approach to extracting the Martin and Braginskii switch resistance with field dependent carrier recombination from measured data.

I. INTRODUCTION

Switches are a critical component in new pulsed power technologies that are seeking to enhance system performance and attain extreme changes in operational regimes. Furthermore, new technologies utilizing more modular approaches such as Protogen [1] or linear transformer driver (LTD) [2] based systems (Ursa Minor [3], Mykonos [4], or the next generation of the Z machine [5]) are heavily dependent upon the synchronized operation of hundreds to thousands of gas insulated pulsed power switches.

Simultaneous operation of many switches is a challenging problem in itself with sensitivity to variations in the manufacturing process, trigger resistor impedance variations due to manufacturing and aging, as well as variations in trigger generator performance when multiple trigger generators are operated in parallel. These variations result in changes to differences in electric field stresses from switch to switch which can dramatically impact jitter and runtime. This impacts efficiency and energy density of pulsed power systems.

Output pulse shaping through precision control of switch closing time is a technique that continues to be refined for dynamic materials research [1]. Systems such

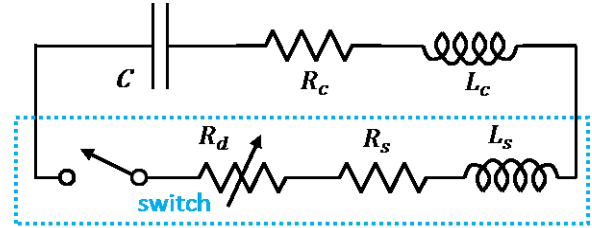


Figure 1. The switch circuit and idealized components. All are assumed constant except R_d .

as Protogen [1] and the Z machine [6], [7] have demonstrated such capabilities however changes in field level for switches that are delayed in time exacerbates the increase of jitter and run time. Techniques that avoid using switch control to define output pulse shape have been demonstrated in systems such as Veloce [8] but with limited success in obtaining a wide range of pulse shapes with variations not only in rise time but also in the shape of the peak and the falling edge of the waveforms.

This paper presents results on characterization of a modified High Current Electronics Institute (HCEI) LTD 200 kV gas switch [9] over a large range of operating conditions. The equivalent circuit diagram representing the test setup for collecting the switch data is provided in Figure 1. A photograph of the two stage Marx consisting of the switch, two 100 kV, 80 nF capacitors, and a low impedance load (CVR) is in Figure 2. In this fixture both the voltage across the capacitor and the current through the switch are measured.

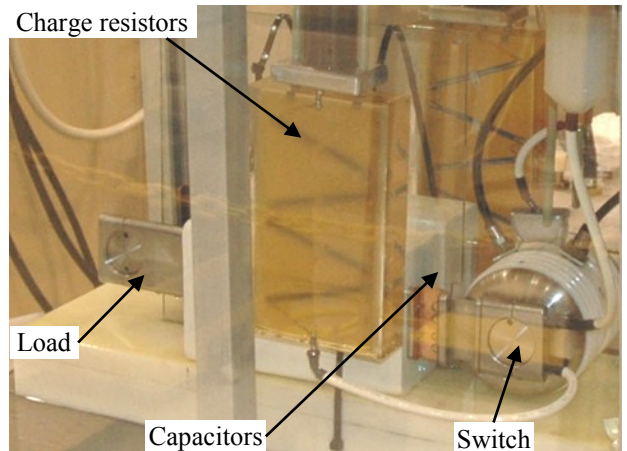


Figure 2. The brick configuration of the test circuit.

* Sandia National Laboratories is a multi-program laboratory managed and operated by Sandia Corporation, a wholly owned subsidiary of Lockheed Martin Corporation, for the U.S. DOE's National Nuclear Security Admin. under contract DE-AC04-94AL85000, SAND Number: 2013-4767 C

✉ email: fjzutav@sandia.gov

U.S. Government work not protected by U.S. copyright

In previous papers, data from this circuit was fit using the Braginskii [10] - Martin [11] model with (1) genetic optimization [12], and (2) piecewise constant resistance least squares fits (LSFs) to a damped harmonic oscillator solution [13]. The genetic optimization gave reasonable fits, but was time intensive (hours on one PC). Piecewise LSFs were much faster (~30s). With this approach, the time period for the current was divided into quarter period intervals (~150 ns), and each interval was fit using constant switch resistance and inductance. The best fit switch resistance was then plotted for each interval, displaying a slowly varying resistance. However, the piecewise fit provided very limited time resolution of the dynamic switch resistance, because the intervals must be relatively large to get reasonable fits to the current. Since switch resistance changes very rapidly as the switch closes (at early time), a higher resolution solution was desired. Both approaches could also be improved by including more realistic plasma behavior such as: field-dependent carrier generation, carrier recombination, and carrier density non-uniformities. In this paper, a least squares fit is made to the current in the differential equation of state (DES) using a modified Braginskii-Martin model for the switch resistance that includes electric field dependent carrier generation and carrier recombination in a cylindrical switch plasma channel with changing diameter. Then a numerical solution is calculated for the current using the fit coefficients for the DES. This provides a single, high resolution, time-dependent solution to the current with dynamic switch resistance that decreases rapidly at early times and increases slowly at late times as the current decays.

II. SWITCH MODEL

The switch model chosen to represent the performance of the HCEI switch is based on spark channel work by Braginskii [10] and switch loss work by Martin [11]. It uses a time varying resistance to describe the energy loss in the switch. This particular model has the advantage of being simplistic in form thereby enhancing the efficiency of system current shaping optimization algorithms. In this model the radius of the spark channel, a , is a function of the current flowing through the channel as defined by

$$a = \sqrt{\left[\frac{4}{\pi^2 \rho_0 \xi \sigma}\right]^{1/3} \int_0^t I^{2/3} dt'} \quad (1)$$

where I is the magnitude of the current in the channel, ρ_0 is the gas density, σ is the conductivity of the gas, and ξ is set to a constant value of 4.5 as defined in [11]. The resistance of a single channel

$$R_{ch} = \frac{l_{ch}}{\sigma \pi a^2} \quad (2)$$

is then based on the radius, where l_{ch} is the channel length. From R_{ch} the total HCEI dynamic switch resistance is calculated as

$$R_d(I, t) = \frac{R_{ch} \left(\frac{I}{n_{ch}}\right)}{n_{ch}} = \frac{R_{ch}(I)}{(n_{ch})^{1/3}} \quad (3)$$

where n_{ch} is the total number of spark channels formed.

If switch inductance and all other circuit/component values are considered constant except the dynamic switch resistance, R_d , then the DES describing the voltage across the ideal switch represented in Figure 1 is

$$V_0 = (L_c + L_s) \frac{dI}{dt} + (R_c + R_s + R_d(I, t))I + \frac{\int_{t_0}^t I dt'}{C} \quad (4)$$

where subscripts C and S stand for fixed circuit/component and switch values, V_0 is the initial voltage across the capacitor, and t_0 is the switching start time. The dynamic resistance is approximated by

$$R_d(I, t) = \frac{\alpha_r}{n_{ch}^{1/3} \left(\frac{n(t)}{n_0}\right)^{2/3} \int_{t_0}^t (I(t'))^{2/3} dt'} \quad (5)$$

where n_0 and $n(t)$ are the initial and temporal ion number densities with $\sigma(t) = n(t)e\mu$ and the constant

$$\alpha_r = \frac{l}{(n_0 e \mu)^{2/3} (4\pi / (\rho_0 \xi))^{1/3}} \quad (6)$$

The Braginskii-Martin models assume temporally constant conductivity in the gas. In this paper, the ion density in the switch channel is modeled as a function of the electric field governed by the rate equation with terms for avalanche generation and carrier recombination with the following constraints.

$$\frac{\dot{n}}{n} = f(E(t)) = \begin{cases} -\frac{1}{\tau_r} & \text{for } E = 0 \\ 0 & \text{for } E = E_0 \\ \frac{1}{\tau_a} & \text{for } E = E_a \gg E_0 \end{cases} \quad (7)$$

$E(t)$ is the magnitude of the electric field in the channel

E_0 is the field at which $\dot{n}=0$ (balanced)

τ_r is the zero field exponential recombination time

τ_a is the high field exponential carrier generation time

E_a is the field at which $f(E_a) = 1/\tau_a$

The general solution for the ion number density is

$$n(t)/n_0 = e^{\int_{t_0}^t f(E(t')) dt'} \quad (8)$$

The electric field dependence of the rate equation, $f(E(t))$, was modeled four ways: linear, quadratic, exponential, and hyperbolic (Figure 3). Only the quadratic and hyperbolic models could fit estimated values for the three constraints in equation (7) ($\tau_r \sim 10^{-6}$ s, $\tau_a \sim 10^{-9}$ s, $E_0 \sim 2.1 \times 10^5$ V, $E_a \sim 2.5 \times 10^5$ V). To do this, the quadratic model went to a negative minimum between $E = 0$ and E_0 which is unphysical. Hence the most appropriate model was the hyperbolic.

$$f(E) = a + \frac{b}{E_b - E} \quad (9)$$

$$E_b = \frac{E_a E_0 \tau_r}{E_0 \tau_r + E_0 \tau_a - E_a \tau_a}, \quad a = \frac{E_b}{E_0 \tau_r}, \quad b = \frac{E_b(E_b - E_0)}{E_0 \tau_r} \quad (10)$$

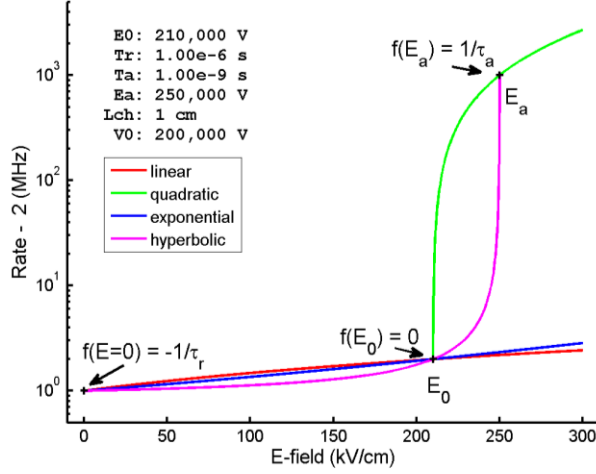


Figure 3. Rate equation models for a 200 kV switch.

The electric field in the switch channel is approximated with the state equation 4 using an initial estimate for the fixed switch inductance and resistance.

$$E(t) \approx \frac{V_0 - (L_C + L_{S0})\dot{I} - (R_C + R_{S0})I - \int I dt'}{l_{ch}} \quad (11)$$

The DES was fit with the initial estimates. Then the results were substituted and the fit was iterated. Stable values were reached in 2 iterations.

III. ANALYSIS OF RESULTS

The current in the switch circuit (Figure 4) was measured with a high bandwidth current viewing resistor (CVR). Digital noise in these measurements was reduced by filtering the data with a low pass filter (Butterworth 30-50 MHz passband-stopband). Substituting equations 11, 9, 8, and 5 into the DES (4), produces a system of approximations for each current data point with three unknown linear coefficients: L_S , R_S , α_r . The sum of the squared residuals in these approximations due to noise can be minimized by solving for unique values of these coefficients using least squares fitting (LSF).

The fixed component values, C , R_C , and L_C , were measured using a precision impedance analyzer. The values used for these calculations were 37.52 nF, 200 mΩ, and 200 nH. Other constants in these equations, n_{ch} , τ_r , τ_a , E_a , E_0 , t_0 , t_{f0} , I_{b0} , were estimated and adjusted manually to minimize the residuals in the fit. (t_0 is the switching start time, t_{f0} is the filter start time, I_{b0} is the current baseline offset.) Including any of these constants as fitting parameters will require a non-linear LSF, due to the dynamic resistance dependence on current (equation 5). The convergence of such non-linear LSF may be tested in future analyses.

A 200 kV switching example is shown in Figure 4. The raw (red dots) and filtered data (red line) are compared to solutions to the DES for 3 different LSFs: (1) fixed resistance, (2) constant resistivity, and (3) dynamic radius and resistivity. Forcing a fixed switch resistance (green),

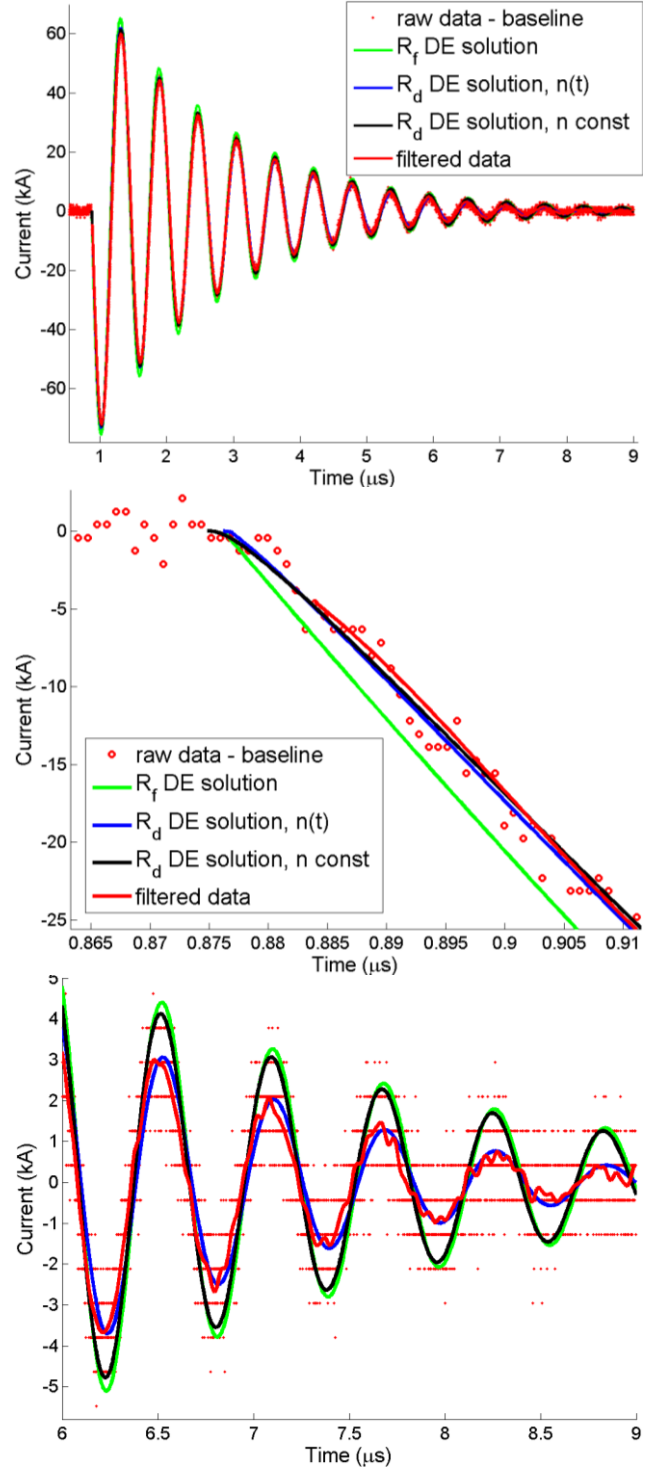


Figure 4. The circuit current for a 200 kV example is measured with a high bandwidth CVR and shown full scale (top), early time enlarged (middle), and late time enlarged (bottom) as raw data (red dots), filtered data (red), and the solutions to the DES with: (1) fixed switch resistance (green), (2) dynamic switch resistance, constant ion number density (black), and (3) dynamic switch resistance, hyperbolic ion number density (blue).

in the fit, results in a current that starts abruptly from zero with a magnitude that is too large at the beginning and the end of the pulse. Allowing a dynamic switch resistance and constant ion number density (black), in the fit, improves agreement near switching initiation, but has too large a magnitude near the end of the pulse. The best fit was achieved with dynamic resistance and the hyperbolic ion number density (blue). Both fits using dynamic resistance start smoothly from zero current.

The fit coefficients and the dynamic resistance from the example shown in Figure 4 are shown in Figure 5 with their 95% confidence intervals of uncertainty. The enlargement (bottom) shows the current periodicity in the dynamic resistance. Note the initial fall in resistance the model predicts with the sudden increase in current. The analytic models for channel diameter and the ion number

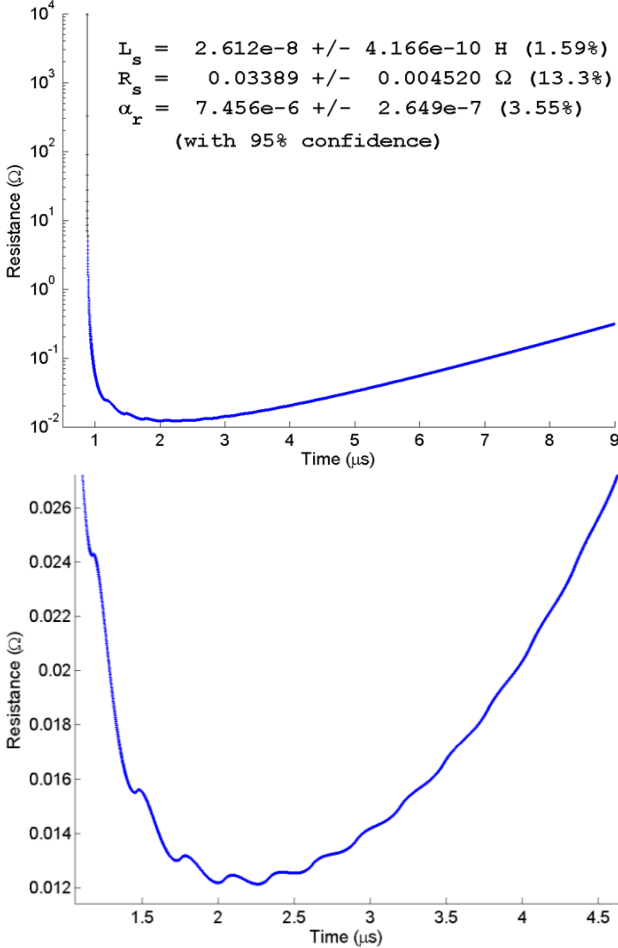


Figure 5. The dynamic resistance was calculated using the modified Braginskii-Martin model with hyperbolic field-dependent ion number density to fit the DES.

density provide solutions with smooth current turn-on as the switch closes. This solution was insensitive to the avalanche carrier generation time, as the effective bandwidth, ~ 500 MHz, and oscillation frequency, ~ 1.7 MHz, of the data are too small to measure sub-nanosecond phenomena associated with sudden switch

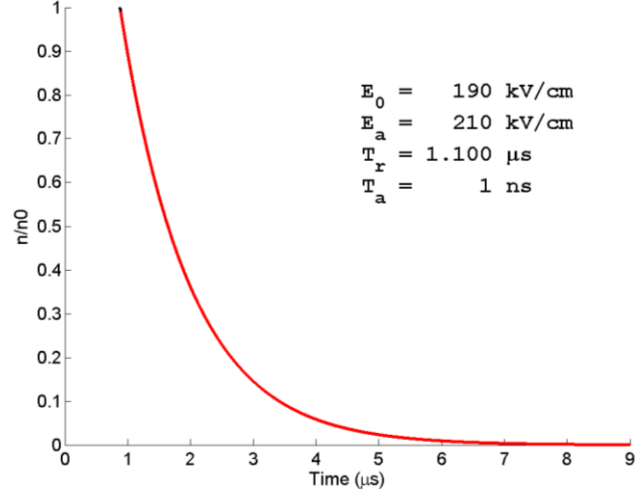


Figure 6. The normalized ion number density calculated for the example shown in the previous figures. While the fit to the data was very sensitive to the recombination time, τ_r , it was insensitive to the avalanche carrier generation time, τ_a .

closure. The late time resistance increase is very sensitive to carrier recombination as the field in the switch channel decreases. The normalized ion number density for this example is shown in Figure 6.

Indications for the quality of the fit to the DES voltage and the quality of the DES solution for current are displayed in Figure 7. The voltage residuals settle quickly from the initial switch closure to less than 2% of the initial voltage, 200 kV. Residuals for the current using dynamic resistance with hyperbolic ion number density are shown relative to the raw data (red dots) and the filtered data (red line). The filtered residuals also settle quickly to less than 2% of the initial current (70 kA). At late time, they are small compared to the noise in the raw data. Also plotted are the residuals for the current using fixed resistance relative to the filtered data (green line). These match the dynamic resistance results in the middle of the time range, but are much larger near the beginning and end of switching. The adjusted R-square (normalized measure of the quality of fit) for this solution based on the current residuals was 0.995 (a perfect fit would be 1).

To assess the reproducibility of these results, 6 shots at 200 kV initial switch voltage and the same pressure were analyzed. The switch resistance, $R_d + R_s$, for each shot is compared in Figure 8. The example in the preceding discussion and figures is the red curve (shot 43) in these plots. The coefficients in the state equation, inductance, L_s , and dynamic resistance, α_r , of the switches are provided in table I along with the total resistance minima, R_m , and start times, t_0 . The top plot in this figure displays the dynamic resistance over the full time range, $\sim 8 \mu\text{s}$.

The other plots in Figure 8 are enlargements which show an early time interval (middle) and an interval containing the resistance minima (bottom). The initial range of variation in time (0.4 ns) is due to scope shot-to-

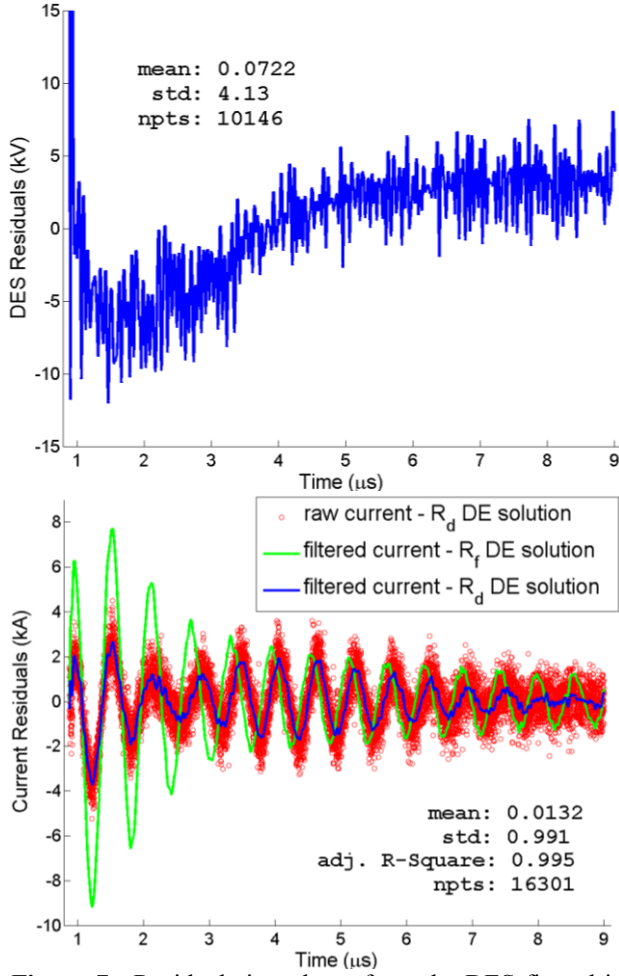


Figure 7. Residuals in voltage from the DES fit and in current from the DES solutions are plotted for the example in the previous figures.

shot sampling synchronization, as the sampling period is 1.3 ns. Timing jitter was removed by basing start times (see t_0 in Table I) on the maximum of the 2nd derivative of the filtered data. The linear segments in this plot are due to the linear extrapolation of the current derivative back in time to the time when the smoothed current was zero. The standard deviation in the resistance minima (2 m Ω) is very small when compared to the overall range in the switch resistance calculation, 10 k Ω (top), and the amplitude noise in this data, ~ 2 kA out of 160 kA peak-to-peak (Figure 4).

The variation in the total switch resistance as a function of the initial switch voltage at the pressure to hold-off 200 kV is shown in Figure 9 and Table II. The minimum total switch resistance, R_m , (bottom) and run time (delay from trigger, t_0 in Table II) decrease with increasing charge voltage. Initial range of time and amplitude variation is similar to the variation shown Figure 8 (middle).

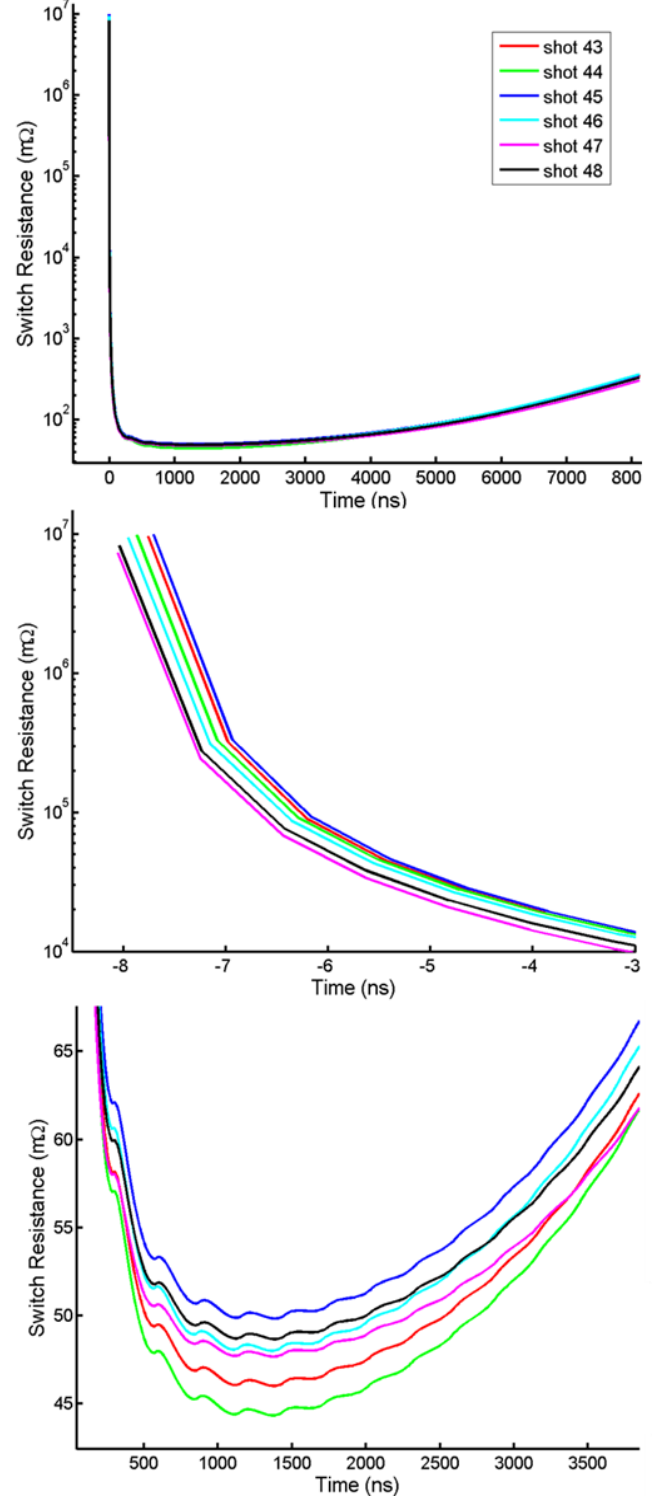


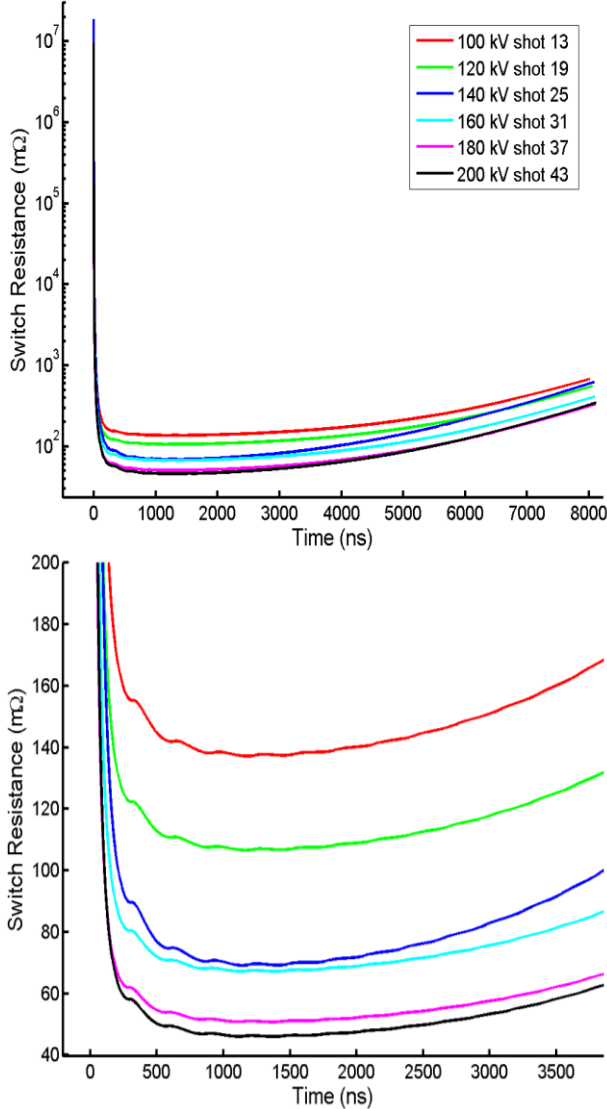
Figure 8. Comparison of the total switch resistance, $R_s + R_d$, calculated for 6 shots at 200 kV. The top plot shows the full scale of calculation. The middle plot is an enlargement of the onset of switching. The bottom is an enlargement of the interval containing the resistance minima.

Table I. The fit coefficients for six shots at 200 kV.

shot	43	44	45	46	47	48	mean	std. dev.
R_m (m Ω)	46	44.3	49.8	48	47.7	48.7	47.4	1.96
L_s (nH)	26.1	23.8	28.5	21.4	25.9	28.7	25.7	2.80
α_r ($\times 10^6$)	7.46	7.78	7.54	7.71	6.32	6.93	7.29	0.560
t_0 (ns)	884	886	885	886	887	886	886	1.13

Table II. The fit coefficients for a range of initial charge voltages.

Voltage (kV)	100	120	140	160	180	200	mean	std. dev.
R_m (m Ω)	137	107	69.2	67.2	50.8	46	79.5	35.4
L_s (nH)	55.8	48.4	37.6	31.4	23.5	26.1	37.1	12.8
α_r ($\times 10^6$)	7.52	7.24	10.2	7.13	6.38	7.46	7.66	1.32
t_0 (ns)	989	943	911	902	894	884	921	39.3

**Figure 9.** Total switch resistance versus charge voltage.

IV. CONCLUSIONS

The Braginskii and Martin switch resistance with field-dependent carrier recombination was extracted from measured data by utilizing least squares fitting and solving the differential equation of state. Modeling the

switch performance as a function of current magnitude, spark channel radius, avalanche generation, and carrier recombination improved the prediction of switch performance from the closing through the opening process. Both the dynamic switch resistance and run time were observed to decrease with increases in the initial charge voltage.

V. ACKNOWLEDGEMENTS

The authors would like to thank the late Dillon McDaniel for his insight and guidance regarding this research.

VI. REFERENCES

- [1] S.F.Glover, et al, "Status of Protogen the 1st integration of Genesis technologies," *PM Conf.*, San Diego, Ca., June, 2012, 641-644.
- [2] A.A. Kim, et al., "100ns Current rise time LTD stage," *PPPS Conf.*, vol. 2, June 2001, pp. 1491-1494.
- [3] J. Leckbee, et al, "Linear Transformer Driver (LTD) research for radiographic applications", *18th IEEE Int. PP Conf.*, Chicago, Il., June, 2011, 614-618.
- [4] W. E. Fowler, et al, "Operating the first water-insulated Mykonos II LTD voltage adder", *17th Int. Symposium on High Current Electronics*, Tomsk, Russia, Sept. 16-21, 2012.
- [5] W.A. Stygar, et al, "Shaping the output pulse of a linear-transformer-driver module", *Physical Review Special Topics – Accelerators and Beams*, 12, 030402 (2009)
- [6] J.P.Davis, et al., "Magnetically driven isentropic compression to multimegabar pressures using shaped current pulses on the Z accelerator," *Physics of Plasmas*, vol. 12, no. 5, 2005.
- [7] C.A.Hall, "Isentropic compression exp. on the SNL Z accelerator," *Physics of Plasmas*, Vol. 7, No. 5, 2069-2075, May 2000.
- [8] T.Ao, et al., "A compact strip-line pulsed power generator for isentropic compression experiments," *Review of Scientific Instruments*, 79, 013903, 2008.
- [9] B.M.Kovalchuk, et al. "Multi gap switch for Marx generators," *PPPS Conf.*, June, 2001, 1739-1742.
- [10] S.I.Braginskii, "Theory of the Development of a Spark Channel," *JETP*, Vol. 34 (7), No. 6, 1068, December 1958.
- [11] T.H.Martin, et al., "Energy Losses in Switches," *9th IEEE Int. PP Conf.*, 463-470, June 1993.
- [12] S.F.Glover, et al., "Status of Genesis: A 5 MA Prog. PP Driver," *18th IEEE Int. PP Conf.*, Chicago, Il., June, 2011, 1309-1314.
- [13] S.F.Glover, et al., "Pulsed power switch modeling for broad operation," *PM Conf.*, San Diego, Ca., June, 2012, 780-783.